High Resolution X-ray Structures of Different Metal-Substituted Forms of Phosphotriesterase from *Pseudomonas diminuta*[†,‡]

Matthew M. Benning,[⊥] Hyunbo Shim,[§] Frank M. Raushel,[§] and Hazel M. Holden*[,⊥]

Department of Biochemistry, University of Wisconsin, Madison, Wisconsin 53706, and Department of Chemistry, P. O. Box 30012, Texas A&M University, College Station, TX 77842-3012

Received November 20, 2000; Revised Manuscript Received January 4, 2001

ABSTRACT: Phosphotriesterase, isolated from the soil-dwelling bacterium *Pseudomonas diminuta*, catalyzes the detoxification of organophosphate-based insecticides and chemical warfare agents. The enzyme has attracted significant research attention in light of its possible employment as a bioremediation tool. As naturally isolated, the enzyme is dimeric. Each subunit contains a binuclear zinc center that is situated at the C-terminal portion of a "TIM" barrel motif. The two zincs are separated by ∼3.4 Å and coordinated to the protein via the side chains of His 55, His 57, His 201, His 230, Asp 301, and a carboxylated Lys 169. Both Lys 169 and a water molecule (or hydroxide ion) serve to bridge the two zinc ions together. Interestingly, these metals can be replaced with cadmium or manganese ions without loss of enzymatic activity. Here we describe the three-dimensional structures of the Zn^{2+}/Zn^{2+}-, Zn^{2+}/Cd^{2+}-, Cd^{2+}/Cd^{2+}-, and Mn^{2+}/Mn^{2+}-substituted forms of phosphotriesterase determined and refined to a nominal resolution of 1.3 Å. In each case, the more buried metal ion, referred to as the α-metal, is surrounded by ligands in a trigonal bipyramidal ligation sphere. For the more solvent-exposed or *β*-metal ion, however, the observed coordination spheres are either octahedral (in the Cd^{2+}/Cd^{2+}-, Mn^{2+}/Mn^{2+}-, and the mixed Zn^{2+}/Cd^{2+}-species) or trigonal bipyramidal (in the Zn^{2+}/Zn^{2+}-protein). By measuring the anomalous X-ray data from crystals of the Zn^{2+}/Cd^{2+}-species, it has been possible to determine that the α-metal ion is zinc and the *β*-site is occupied by cadmium.

Phosphotriesterase, isolated from the soil-dwelling bacterium *Pseudomonas diminuta*, catalyzes the hydrolysis of organophosphate nerve agents (*1*−*2*). The reaction, illustrated with the insecticide paraoxon, is depicted in Scheme 1. In addition to the commonly employed organophosphorus-based pesticides, the enzyme has also been shown to catalyze the detoxification of chemical warfare agents such as sarin (GB), soman (GD), and VX (*3*).

Both EPR and NMR data have demonstrated that each subunit of the dimeric enzyme contains two divalent metal ions which, in the naturally occurring protein, are zinc ions (*4*−*5*). Interestingly, the two zincs can be replaced with Cd^{2+}, Ni^{2+}, Co^{2+}, and Mn^{2+} ions without loss of enzymatic activity (*6*). Specifically, using paraoxon as the substrate, the value of k_{cat} for the Co^{2+}/Co^{2+}-containing enzyme is the fastest, followed by the Ni^{2+}/Ni^{2+}-, Cd^{2+}/Cd^{2+}-, Zn^{2+}/Zn^{2+}-, and Mn^{2+}/Mn^{2+}-substituted proteins (*6*).

From X-ray crystallographic analyses, each subunit is known to adopt a "TIM" barrel motif with the binuclear metal center located at the C-terminal portion of the *β*-barrel (*7*−*9*). In the wild-type enzyme, the two zinc ions are ligated to the protein through the side chains of a single aspartate (Asp 301) and four histidines (His 55, His 57, His 201, and His 230). In addition, the two metal ions are bridged together by a carbamate functional group, formed by the carboxylation of Lys 169, and a water (or hydroxide ion) from the solvent. As illustrated in Figure 1, the ligation geometry of the binuclear metal center in phosphotriesterase closely resembles the binuclear Ni^{2+} center observed in urease (*10*).

Scheme 1

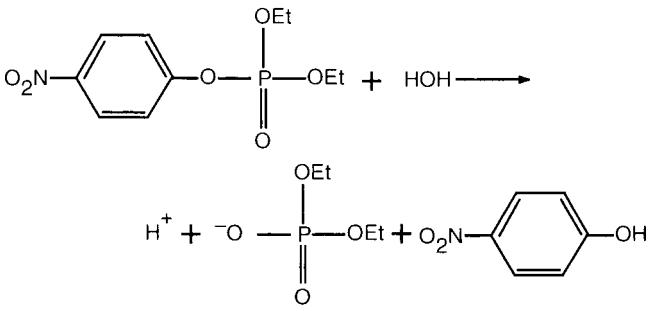

A stereochemical analysis of the overall reaction catalyzed by phosphotriesterase has demonstrated that the phosphorus-containing product is formed with a net inversion of configuration (*11*). This result rules out the formation of a phospho-enzyme intermediate, and thus the reaction mechanism occurs most likely via the attack of the bridging water or hydroxide directly on the phosphorus center of the bound

[†] This research was supported in part by NIH Grants GM-33894 (to F.M.R.) and GM-55513 (to H.M.H.).

[‡] X-ray coordinates have been deposited in the Research Collaboratory for Structural Bioinformatics, Rutgers University, New Brunswick, N. J. (1HZY), (1IO3), (1IOB), and (1IOD) and will be released upon publication.

* To whom correspondence should be addressed. E-mail: Hazel_Holden@biochem.wisc.edu. Fax: 608-262-1319. Phone: 608-262-4988.

[⊥] University of Wisconsin.

[§] Texas A&M University.

10.1021/bi002661e CCC: $20.00
Published on Web 02/06/2001

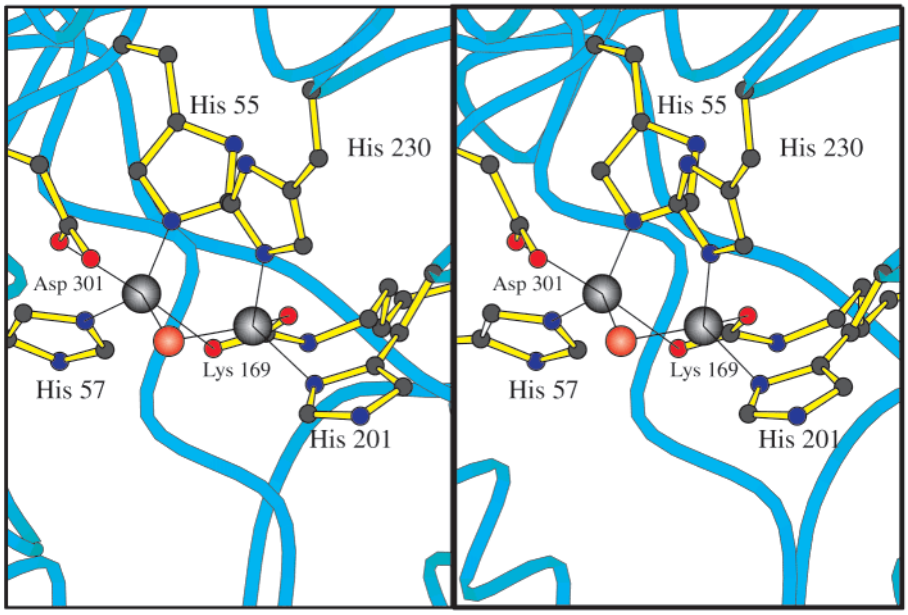

FIGURE 1: Close-up view of the binuclear metal center located in the active site of phosphotriesterase. This figure, and Figures 4−7 were prepared with the software package, MOLSCRIPT (*21*). X-ray coordinates utilized for this figure were determined in this laboratory and can be obtained from the Protein Data Bank (1DPM). The two zinc ions are shown as large gray spheres with the position of the bridging water or hydroxide ion indicated by the large red sphere. The structure presented here was solved in the presence of a substrate analogue, diethyl 4-methylbenzyl phosphonate (not shown), and as such the β-metal is tetrahedrally ligated. Coordinate covalent bonds between the metals and the ligands are indicated by the black lines.

substrate. The precise roles that each of the two divalent cations play in the catalytic process are not entirely clear. These two metal ions may function singly or in concert to lower the pK_a of the bridging solvent molecule. The divalent cations may also polarize the phosphoryl oxygen bond of the substrate to make the reaction center more electrophilic. Additionally, one or both of these metal ions may serve to neutralize the distribution of negative charge on the leaving group as the reaction progresses.

The differential roles in binding and catalysis, played by the two divalent cations within the binuclear metal center of phosphotriesterase, have been probed by X-ray diffraction studies and the preparation of a unique mixed-metal hybrid enzyme. Recent X-ray crystallographic studies of phosphotriesterase have indicated that the more solvent-exposed or β-metal ion is within 2.5 Å of the phosphoryl oxygen of the non-hydrolyzable inhibitor, diisopropyl methyl phosphonate, bound to the active site (*12*). This metal ion is thus poised to polarize the P═O bond of a true substrate for nucleophilic attack. The mixed-metal Zn^{2+}/Cd^{2+}-species of phosphotriesterase has been prepared, and the catalytic properties of this unique hybrid most closely resemble those of the Zn^{2+}/Zn^{2+}-phosphotriesterase (*5*). Therefore, it appears that one of the two metal ions may dominate the catalytic steps that govern the magnitude of k_{cat} and k_{cat}/K_m during the hydrolysis of paraoxon. ^{113}Cd-NMR spectroscopy of the Zn^{2+}/Cd^{2+}-phosphotriesterase hybrid has demonstrated that only one of the two possible hybrid complexes is formed, but the assignment of a specific metal ion to an individual binding site has not been possible thus far (*5*).

Here we report the high-resolution X-ray structures of the Zn^{2+}/Zn^{2+}-, Cd^{2+}/Cd^{2+}-, Mn^{2+}/Mn^{2+}-, and Zn^{2+}/Cd^{2+}-substituted forms of phosphotriesterase crystallized in the absence of substrate analogues. These X-ray crystal structures were solved to a nominal resolution of 1.3 Å to provide greater molecular insight into the perturbations imposed on the binuclear metal center and the surrounding active site through the occupancy of metal ions of various radii and charge densities. Additionally, by measuring the anomalous X-ray data from crystals of the Zn^{2+}/Cd^{2+}-substituted species, it has been possible to assign the individual divalent cations to the two specific α- and β-metal binding sites.

MATERIALS AND METHODS

Crystallization and X-ray Data Collection. Crystals of the various substituted forms of phosphotriesterase were grown according to previously published procedures with the only modification being the replacement of 1% (v/v) diethyl 4-methylbenzylphosphonate with 1% (v/v) 2-phenylethanol (*8*). All of the crystals belonged to the space group *C*2 with typical unit cell dimensions of $a = 129.5$ Å, $b = 91.4$ Å, $c = 69.4$ Å, $\beta = 91.9°$ and two subunits per asymmetric unit.

For X-ray data collection, the crystals were first serially transferred to cryoprotectant solutions of a synthetic mother liquor containing 6, 12, 18, and 23% ethylene glycol. The synthetic mother liquor was composed of 14% (w/v) poly(ethylene glycol) 8000, 200 mM NaCl, 0.5% (v/v) 2-phenylethanol, and 50 mM CHES (pH 9.0).[1] Each crystal was then flash-cooled to −150 °C in a stream of nitrogen gas and subsequently stored under liquid nitrogen until synchrotron beam time became available.

Each X-ray data set was collected on a 3 × 3 tiled "SBC2" CCD detector at the Structural Biology Center 19-ID Beamline (Advanced Photon Source, Argonne National Laboratory). The X-ray data were processed with DENZO and scaled with SCALEPACK (*13*). Relevant X-ray data collection statistics are presented in Table 1.

Structural Analyses. All of the structures presented here were solved by Difference Fourier techniques. Each model

[1] Abbreviations: bicine, *N*,*N*-bis(2-hydroxyethyl)glycine; CHES, 2-(cyclohexylamino)ethanesulfonic acid.

Table 1: X-ray Data Collection Statistics

	Zn^{2+}/Zn^{2+}	Cd^{2+}/Cd^{2+}	Mn^{2+}/Mn^{2+}	Zn^{2+}/Cd^{2+}
resolution range (Å)	30.0−1.3	30.0−1.3	30.0−1.3	30.0−1.3
integrated reflect.	1 448 033	1 231 444	1 367 510	1 626 798
independent reflect.	186 115	187 426	184 739	190 056
data completeness (%)	97 (97)	98 (99)	96 (99)	99 (99)
avg I/avg $\sigma(I)$[a]	25 (4.0)	32 (8.0)	21.6 (4.3)	30.3 (2.8)
R_{sym} (%)[a]	9.6 (17.3)	6.9 (18.4)	9.2 (23.3)	5.8 (31.0)

[a] $R_{sym} = (\sum|I - \bar{I}|/\sum I) \times 100$. The numbers in the parentheses correspond to the resolution range of 1.35 to 1.30 Å.

was subjected to alternate cycles of least-squares refinement at 1.3 Å resolution with the software package TNT (*14*) and manual adjustment with the graphics program TURBO (*15*). Relevant refinement statistics are given in Table 2. Note that the *R*-factors listed in Table 2 are based on all measured X-ray data with no sigma cutoffs applied. In each structural analysis, the electron density corresponding to subunit II was slightly better ordered than that for subunit I. Consequently, the following discussion of the various metal-substituted forms of phosphotriesterase will refer only to subunits II in the X-ray coordinate files unless otherwise indicated. Sodium ions were identified on the basis of both the octahedral coordination geometry of the ligands surrounding them and the bond distances.

Determination of the Metal Binding Positions for the Zn^{2+}/Cd^{2+}-Substituted Enzyme. To determine the exact location of the zinc and cadmium ions in the mixed metal hybrid species of phosphotriesterase, two separate X-ray experiments were conducted. In the first study, an X-ray data set, designed to measure the anomalous scattering from a crystal of the mixed hybrid species, was collected to 1.3 Å resolution at the Advanced Photon Source, Structural Biology Center beamline. This X-ray data set was processed with DENZO and scaled with SCALEPACK (*13*). Protein phases, calculated from the phosphotriesterase model with the metals and solvents removed from the coordinate file, were employed to calculate an anomalous difference electron density map. At an X-ray wavelength of 0.70087, the $\Delta f''$ for zinc is 1.431 and for cadmium is 1.202 (International Tables, Vol. IV). Consequently, the larger peak in the difference anomalous electron density map should correspond to zinc. Integrated peak heights were obtained from MAPMAN (*16*). In subunit I of the asymmetric unit, the integrated intensities for the

Table 2: Least-Squares Refinement Statistics

	Zn^{2+}/Zn^{2+}	Cd^{2+}/Cd^{2+}	Mn^{2+}/Mn^{2+}	Zn^{2+}/Cd^{2+}
resolution limits (Å)	30.0−1.3	30.0−1.3	30.0−1.3	30.0−1.3
R-factor (overall) %/no. of rflns[a]	19.6 (186 115)	20.4 (187 426)	22.5 (184 739)	19.3 (190 056)
R-factor (working) %/no. of rflns	19.6 (176 950)	20.2 (178 183)	22.2 (175 396)	19.1 (180 701)
R-factor (free) %/no. of rflns	22.8 (9165)	23.6 (9243)	26.7 (9343)	22.4 (9355)
no. of protein atoms	5044	5044	5044	5044
multiple conformations	17	18	17	18
	weighted root-mean-square deviations from ideality			
bond lengths (Å)	0.012	0.011	0.011	0.011
bond angles (Å)	2.2	2.1	2.3	2.2
trigonal planes (Å)	0.007	0.006	0.007	0.007
general planes (Å)	0.009	0.008	0.009	0.009
torsional angles (deg)[b]	14.6	14.6	15.0	14.6
	solvents			
waters	692	738	710	737
Na^+ ions	2	2	2	2
ethylene glycols	20	27	26	15
2-phenylethanols	2	2	2	2

multiple conformations

Zn^{2+}/Zn^{2+}	Cd^{2+}/Cd^{2+}	Mn^{2+}/Mn^{2+}	Zn^{2+}/Cd^{2+}
110 VAL	110 VAL	110 VAL	110 VAL
111 SER	111 SER	111 SER	111 SER
159 GLU	196 VAL	196 VAL	156 TYR
196 VAL	222 SER	222 SER	196 VAL
222 SER	295 GLN	238 SER	222 SER
238 SER	298 VAL	241 THR	238 SER
241 THR	359 SER	295 GLN	241 THR
295 GLN	510 VAL	359 SER	295 GLN
359 SER	518 ARG	510 VAL	359 SER
510 VAL[c]	573 THR	511 SER	510 VAL
518 ARG	596 VAL	518 ARG	511 SER
596 VAL	669 SER	622 SER	518 ARG
622 SER	685 LYS	685 LYS	622 SER
669 SER	695 GLN	698 VAL	685 LYS
685 LYS	698 VAL	759 SER	698 VAL
698 VAL	759 SER	810 EG	759 SER
759 SER	810 EG[d]	811 EG	810 EG
	852 PEA[e]		811 EG

[a] *R*-factor $= (\Sigma|F_o - F_c|/\Sigma|F_o|) \times 100$ where F_o is the observed structure-factor amplitude and F_c is the calculated structure-factor amplitude. For calculation of *R*-free, 5% of the X-ray data were removed from the reflection file. [b] The torsional angles were not restrained during the refinement. [c] Amino acid residues with numbers higher than 400 correspond to those found in subunit II (beginning at residue 434). [d] Ethylene glycol is abbreviated as EG. [e] 2-phenylethanol is abbreviated as PEA.

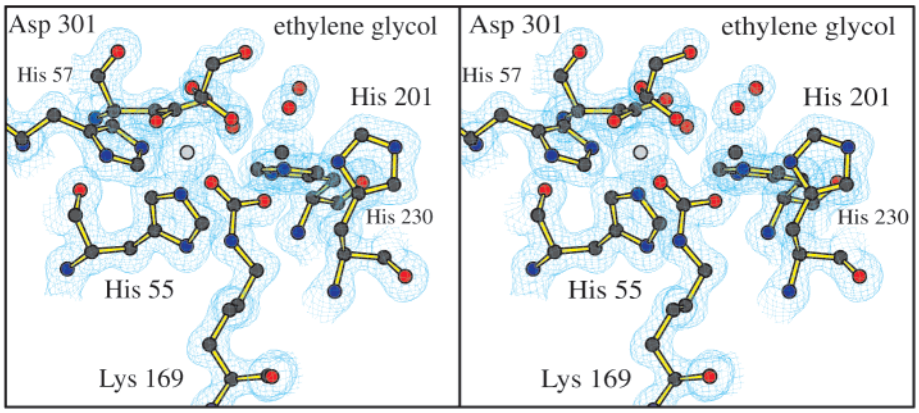

FIGURE 2: Representative portion of the electron density map calculated for the Zn^{2+}/Cd^{2+}-hybrid phosphotriesterase. The electron density displayed was contoured at 1σ and calculated with coefficients of the form $(2F_o-F_c)$, where F_o was the native structure factor amplitude and F_c was the calculated structure factor amplitude. The positions of the zinc and cadmium ions are indicated by the light and dark gray spheres, respectively.

peaks at the α- and β-sites were 30.3 and 25.6, respectively. Likewise, in subunit II, integrated intensities of 35.2 and 29.7 were observed for the α- and β-sites, respectively. These data indicate that the α-metal site is occupied by zinc, while cadmium binds to the β-site.

As further evidence to the identity of the metals occupying the α- and β-sites, a second X-ray data set was collected to 1.9 Å resolution with Cu Kα radiation. The X-ray data were measured with a Proteum/R rotating anode generator/CCD detector system, processed with SaintPlus, and scaled with ProScale (Bruker AXS, Inc., Madison, WI 53711 USA). Again Friedel pairs were measured. At a wavelength of 1.54178 Å, the $\Delta f''$ for zinc is 0.678 and for cadmium is 4.653. In this case, the larger integrated peak intensity should correspond to the cadmium ion. In subunit I of the asymmetric unit, the integrated intensity for the α-site was 31.8 and for the β-site was 34.5, while for subunit II the intensities were 36.1 and 41.0, respectively, for the α- and β-sites. Again these data are indicative of a mixed hybrid species whereby the zinc ion occupies the α-site while the cadmium ion locates to the β-site. A portion of the electron density map near the Zn^{2+}/Cd^{2+}-binuclear metal center is displayed in Figure 2.

RESULTS

Structure of the Zn^{2+}/Zn^{2+}-Containing Phosphotriesterase. A Ramachandran plot of all non-glycinyl ϕ, ψ angles for the Zn^{2+}/Zn^{2+}-containing enzyme is given in Figure 3. As can be seen, the quality of the refined model is outstanding with the only significant outliers being Ser 61, Trp 131, Glu 159, and Asn 312 in both subunits of the dimer. In each case, the electron densities corresponding to the above-mentioned amino acid residues are unambiguous. Ser 61 is located at the end of a β-strand near the C-terminal portion of the "TIM" barrel, while the indole ring of Trp 131 is located within ~5 Å of the binuclear metal center. Both Glu 159 and Asn 312 are located in reverse turns, (type II′ and type II, respectively), which are distant from the active site of the enzyme.

Shown in Figure 4, panel a, is a close-up view of the active site for the Zn^{2+}/Zn^{2+}-containing phosphotriesterase. Only those residues that are located within ~5 Å of the metal-bridging water or hydroxide ion are displayed. All of the

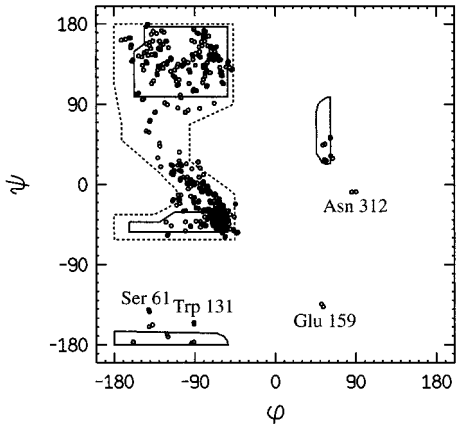

FIGURE 3: Ramachandran plot of all non-glycinyl main chain ϕ, ψ angles. Those dihedral angles that are fully or partially allowed are enclosed by the solid or dashed lines, respectively. All of the models for phosphotriesterase presented here adhere tightly to the allowed regions of the Ramachandran plot.

crystals employed for these high-resolution X-ray analyses described here were grown in the absence of substrate analogues or inhibitors. However, each crystal was transferred to a cryoprotectant solution containing ethylene glycol and, indeed, several ethylene glycols are observed binding in the active site region of the zinc-substituted protein as indicated in Figure 4, panel a. Interestingly, these ethylene glycols occupy similar positions to those observed for the ethoxy groups of triethyl phosphate when this inhibitor is bound to phosphotriesterase (*12*).

The first X-ray structure of the Zn^{2+}/Zn^{2+}-form of phosphotriesterase was solved in the presence of the inert inhibitor, diethyl 4-methylbenzylphosphonate (*9*). In that structure, the zinc ion in the α-site was ligated by His 55, His 57, Lys 169, Asp 301, and the metal-bridging water or hydroxide in a trigonal bipyramidal arrangement. The β-site metal ion, however, was coordinated in a distorted tetrahedral environment via Lys 169, His 201, His 230, and the metal-bridging water or hydroxide ion. Following this X-ray crystallographic analysis, the structure of the zinc-containing enzyme was determined in the presence of either diisopropyl methyl phosphonate (a sarin mimic) or triethyl phosphate (*12*). In both complexes, the α-metal ions adopted similar trigonal bipyramidal coordination spheres. With respect to the zincs occupying the β-sites, however, the two models

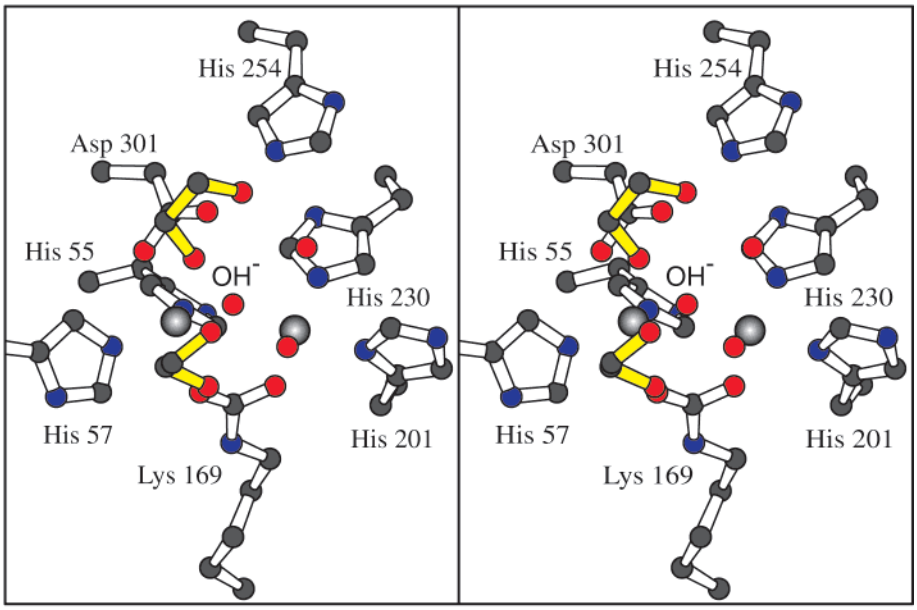

(a)

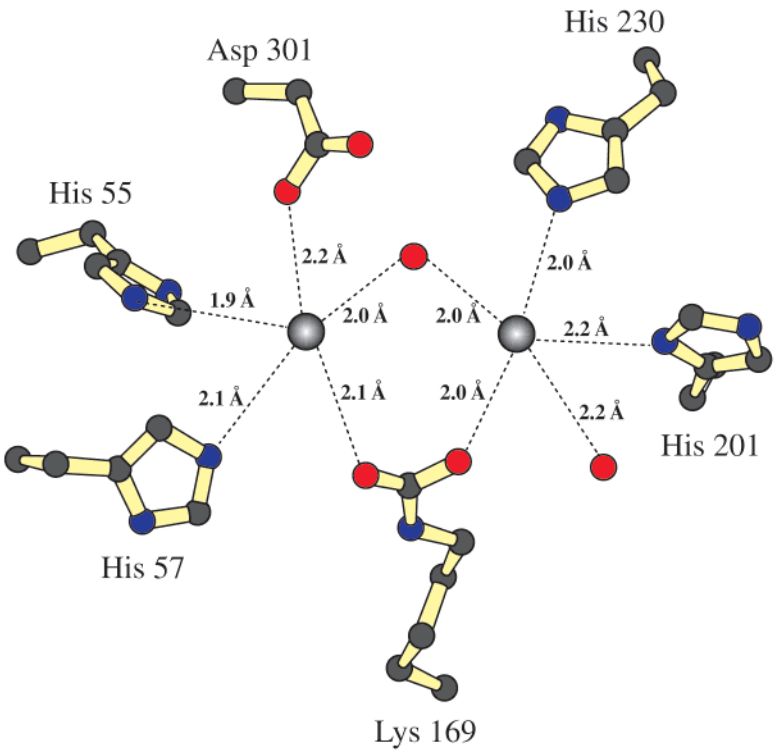

(b)

FIGURE 4: Close-up view of the active site region for the Zn^{2+}/Zn^{2+}-containing enzyme. Those amino acid residues and solvents lying within ~5 Å of the metal-bridging water or hydroxide ion are shown in stereo in panel a. The zinc ions are depicted as gray spheres, while the water molecules are displayed as red balls. Two ethylene glycol molecules, highlighted in yellow bonds, are observed binding within this 5 Å sphere. A cartoon of the coordination geometry for the binuclear metal center is given in panel b. The metal/ligand bond distances are as indicated and are the averaged values observed for the two molecules contained within the asymmetric unit.

differed significantly. For the enzyme−diisopropyl methyl phosphonate complex, the zinc was surrounded in a distorted trigonal bipyramidal ligation sphere by Lys 169, His 201, His 230, the bridging water or hydroxide ion, and the phosphoryl oxygen of the substrate analogue. Indeed, this observed geometry with the inhibitor binding to the zinc ion further supports the proposed catalytic mechanism whereby the phosphorus of the substrate is activated for nucleophilic attack by interaction of the phosphoryl oxygen with a positively charged metal ion. In contrast, for the phosphotriesterase/triethyl phosphate model, the zinc ion was once again observed adopting a tetrahedral coordination sphere.

A cartoon of the observed coordination geometry for the zinc-containing enzyme described here is presented in Figure

4, panel b. Again, the α-site zinc is ligated by His 55, His 57, Asp 301, Lys 169, and the bridging water or hydroxide ion in a distorted trigonal bipyramidal geometry with coordinate covalent bonds ranging in length from 1.9 to 2.2 Å. The axial ligands are provided by the side chain oxygens of Asp 301 and Lys 169, while the equatorial bonds are formed between the metal and His 55, His 57, and the bridging water or hydroxide. The angles observed between an axial ligand, the metal, and an equatorial ligand range in size from 86.0 to 100.2° with an average angle of 90.3° (subunit II). The angles observed between the equatorial ligands and the metal are 114.2° (His 55−Zn^{2+}−His 57), 111.6° (His 55−Zn^{2+}−hydroxide), and 134.2° (His 57−Zn^{2+}−hydroxide). Contrary to that observed for phosphotriesterase solved in the presence of either the bound inhibitor diethyl 4-methylbenzyl phosphonate or triethyl phosphate, the *β*-site zinc ion in the structure presented here is surrounded in a distorted trigonal bipyramidal arrangement with the axial ligands being His 201 and the metal-bridging water or hydroxide ion and the equatorial ligands provided by Lys 169, His 230, and a water molecule. In this case, the angles observed between an axial ligand, the metal, and an equatorial ligand range in size from 77.1 to 99.2° with an average angle of 90.9° (subunit II). The angles observed between the equatorial ligands and the metal are 110.0° (Lys 169−Zn^{2+}−water), 111.3° (Lys 169−Zn^{2+}−His 230), and 138.7° (His 230−Zn^{2+}−water). There is one water molecule located at ∼3.3 Å that if it were positioned somewhat closer could coordinate to the zinc to complete an octahedral ligation sphere. Note that the Zn^{2+} ions, with ionic radii of 0.74 Å, are separated by 3.5 Å (subunit II).

One question that immediately arises is why the *β*-site zinc is tetrahedrally ligated when either triethyl phosphate or diethyl 4-methylbenzyl phosphonate is bound in the active site pocket but is surrounded in a trigonal bipyramidal coordination sphere in the current model. A superposition of the various zinc-containing protein models demonstrates that the phosphoryl oxygens of the inhibitors (triethyl phosphate or diethyl 4-methylbenzylphosphonate) lie within ∼1 Å of where the water molecule (shown in Figure 4, panel b) is situated in the structure presented here. Consequently, these two specific inhibitors effectively exclude water from the zinc ligation sphere thereby reducing the number of coordinate covalent bonds to the metal from five to four.

Structure of the Zn^{+2}/Cd^{+2}-Containing Phosphotriesterase. From $^{113}Cd^{2+}$-NMR spectroscopy, it is known that in the mixed metal hybrid species of phosphotriesterase, the zinc ion occupies one specific site while the cadmium ion is located at the second position in the binuclear metal center (*5*). By measuring the anomalous signal from a crystal of the Zn^{2+}/Cd^{2+}-enzyme hybrid, it has been possible to establish that zinc occupies the α-site position while cadmium locates to the more solvent-exposed *β*-site. The zinc and cadmiums are separated by 3.6 Å (subunit II).

A close-up view of the mixed hybrid binuclear metal center is shown in stereo in Figure 5, panel a, and a cartoon of the coordination geometry is given in Figure 5, panel b. Again, two ethylene glycols are located within 5 Å of the bridging water or hydroxide ion. In this case, however, the oxygen of one of the ethylene glycols adopts two specific orientations as indicated by O1 and O1* in Figure 5, panel a. In the O1 orientation, the oxygen lies within hydrogen bonding distance to the oxygen of the second ethylene glycol moiety. In the O1* case, the oxygen hydrogen bonds to one of the three solvent molecules comprising the ligation sphere for the cadmium ion.

As indicated in Figure 5, panel b, the coordination sphere for the zinc ion is trigonal bipyramidal with Asp 301 and Lys 169 serving as the axial ligands and His 55, His 57, and the bridging water or hydroxide functioning as equatorial ligands. The observed angles are similar to those described for the Zn^{2+}/Zn^{2+}-containing phosphotriesterase. The ligands surrounding the cadmium ion, however, adopt a distorted octahedral configuration with angles ranging in size from 71.9 to 103.3° and an average angle of 89.4° (subunit II).

Structure of the Cd^{+2}/Cd^{+2}-Containing Phosphotriesterase. A close-up view of the active site of this form of phosphotriesterase is depicted in Figure 6, panel a. As observed in the mixed-metal hybrid structure, one of the ethylene glycols observed binding in the active site adopts multiple conformations as indicated by O1 and O1* in Figure 6, panel a. Not surprisingly, and in light of the ionic radius for Cd^{2+} (0.97 Å), the two metals in this complex are slightly more separated (3.7 Å). The α-site cadmium ion is situated in a trigonal bipyramidal environment with the axial ligands being Asp 301 and Lys 169 and the equatorial ligands provided by His 55, His 57, and the bridging water or hydroxide ion. The angles between the axial ligands, the metal, and the equatorial ligands range in size from 84.2 to 99.0° with an average angle of 90.2° (subunit II). The angles between an equatorial ligand, the metal, and another equatorial ligand range from 110.3 to 134.8°. With respect to the *β*-site cadmium ion, the ligands are arranged in a somewhat less distorted octahedral environment, as compared to that observed in the Zn^{2+}/Cd^{2+}-hybrid, with bond angles ranging from 79.8 to 101.6° and an average angle of 89.6° (subunit II). Bond lengths between the metals and the ligands are indicated in the cartoon representation in Figure 6, panel b.

Structure of the Mn^{+2}/Mn^{+2}-Containing Phosphotriesterase. The final structure to be investigated in this study is that of phosphotriesterase with its binuclear metal center containing two Mn^{2+} ions (with ionic radii of 0.80 Å). These ions are separated by 3.7 Å. A stereo representation of the active site is displayed in Figure 7, panel a. In this structure, only one ethylene glycol moiety is positioned within 5 Å of the bridging water or hydroxide ion and does not adopt multiple conformations. As can be seen by comparing Figure 6, panel b, and Figure 7, panel b, the coordination geometries for the two manganese ions are similar to those observed for the cadmiums. For the α-site manganese ion, the angles between the axial ligands, the metal, and the equatorial ligands range from 81.6 to 101.1° with an average angle of 90.2° (subunit II). The angles in the equatorial plane are 107.1, 109.0, and 143.4°. With regard to the manganese occupying the *β*-site, the ligands are again arranged in an octahedral coordination sphere with angles ranging from 80.5 to 98.8° and an average size of 89.8°.

DISCUSSION

The various structural analyses of phosphotriesterase that have been conducted over the last six years have been filled with surprise after surprise. Indeed, the first form of the enzyme to be crystallized was that of the Cd^{2+}/Cd^{2+}-containing protein. The crystals were observed growing from

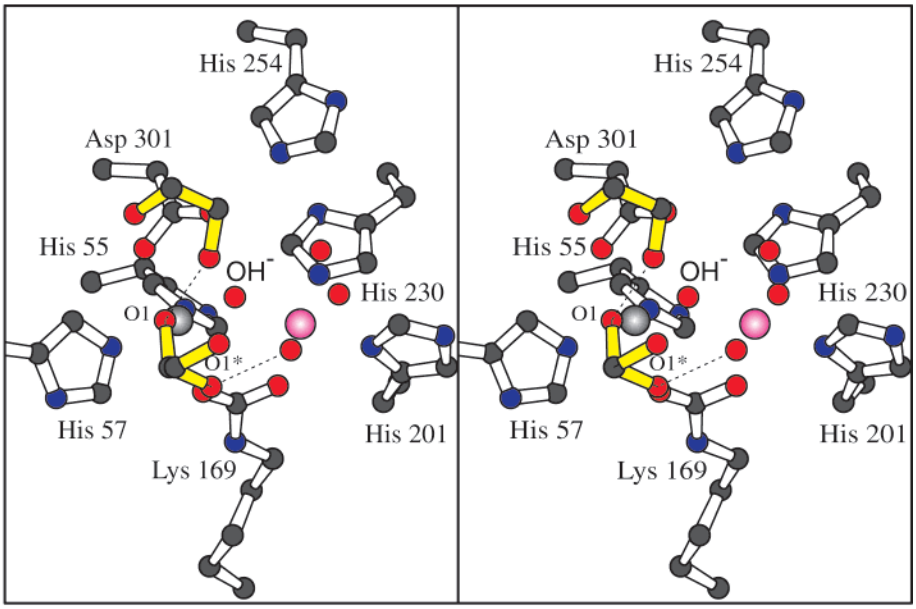

(a)

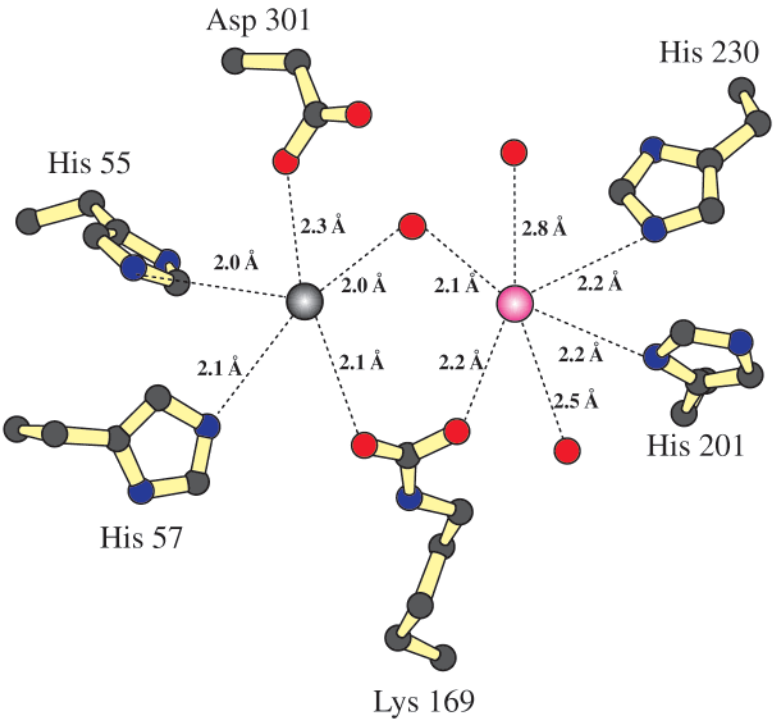

(b)

FIGURE 5: Close-up view of the active site region for the Zn^{2+}/Cd^{2+}-containing enzyme. As can be seen in panel a, two ethylene glycols, highlighted in yellow bonds, are located within 5 Å of the bridging water or hydroxide ion. One of these adopts two different conformations as indicated by the labels, O1 and O1*. The cadmium ion is represented by the pink sphere, while the zinc ion is displayed as a gray sphere. A cartoon of the coordinate covalent bonding pattern around the binuclear metal center is presented in panel b. The metal/ligand bond distances are averaged values observed for subunits I and II.

poly(ethylene glycol) 8000, 100 mM bicine (pH 9.0), and 1 M LiCl (*7*). Inadvertently, these crystallization conditions effectively chelated the binuclear metal center from the active site and the structure solved was that of the apo-enzyme. While unintentional, this initial X-ray crystallographic analysis at least revealed that the overall fold of phosphotriesterase was a "TIM" barrel and that the quaternary structure of the enzyme was dimeric rather than monomeric as had been previously assumed. Subsequently, the structure of the Cd^{2+}/Cd^{2+}-containing enzyme was solved by removing LiCl from the crystallization buffer and utilizing CHES rather than bicine as the buffer. Interestingly, crystals only appeared under these new conditions when diethyl 4-methylbenzyl phosphonate, a substrate analogue, was included in the mother liquor. It was thus tacitly assumed that this inhibitor would be found binding in the active site. While the crystals

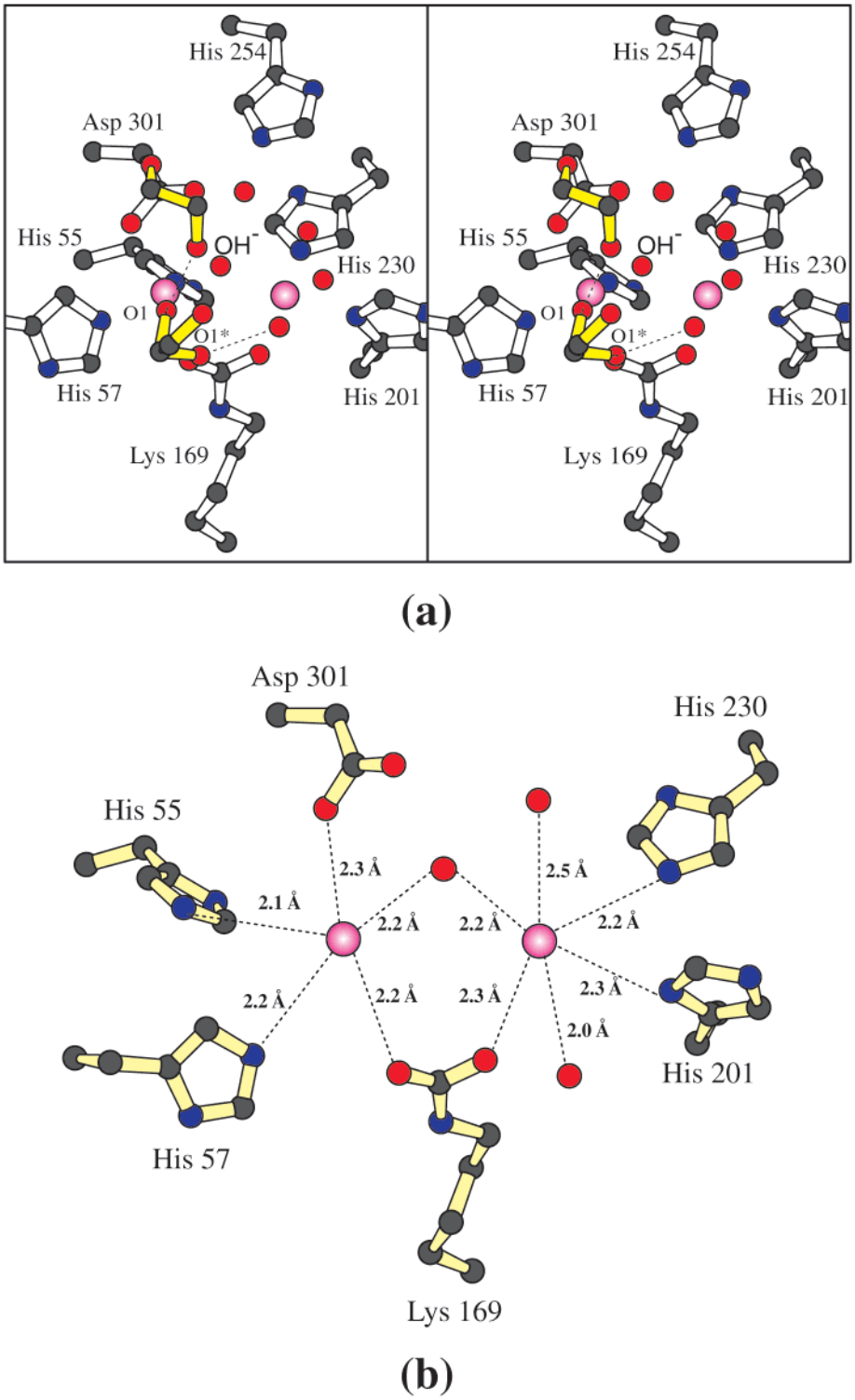

FIGURE 6: Close-up view of the active site region for the Cd^{2+}/Cd^{2+}-containing phosphotriesterase. The two cadmium ions of the binuclear metal center are colored in pink. Like that observed in the zinc/cadmium hybrid, one of the ethylene glycols adopts two specific conformations, O1 and O1*, as indicated in panel a. A schematic of the binuclear metal center is depicted in panel b. The metal/ligand bond distances are averaged values observed for subunits I and II.

grown under these new conditions did, indeed, allow for a structural determination of the holo-enzyme with an intact binuclear metal center, the diethyl 4-methylbenzyl phosphonate was observed binding between two symmetry-related molecules in the crystalline lattice and not in the active site (*8*). Two additional surprises unfolded in this second X-ray structural analysis of phosphotriesterase. First, one of the bridging ligands to the cadmiums was, quite unexpectedly, a carboxylated lysine residue (Lys 169). This residue was not covalently modified in the apo-enzyme structure. Second, the conformations of the polypeptide chains for the apo- and holo-enzymes were quite different such that their α-carbons superimposed with a root-mean-square deviation of 3.4 Å. The changes in backbone conformations between the two forms of the protein were limited to several regions, however, with the most striking difference occurring near Asp 301.

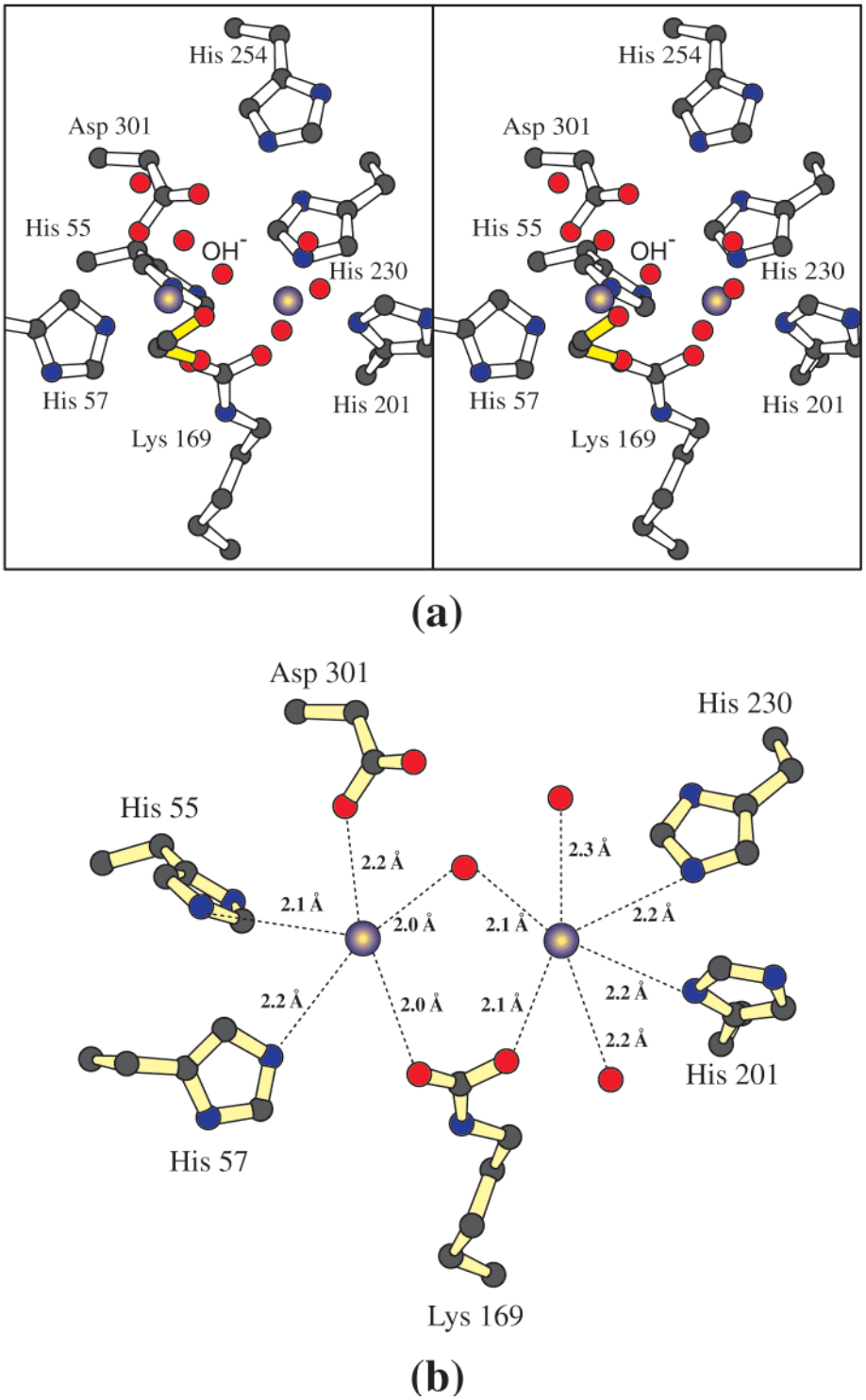

FIGURE 7: Close-up view of the active site region for the Mn^{2+}/Mn^{2+}-substituted protein. A stereoview of the active site is shown in panel a, while a cartoon of the binuclear metal center given in panel b. The manganese ions are depicted as bluish-yellow spheres. The metal/ligand bond distances are averaged values observed for subunits I and II.

In the apo-enzyme, Asp 301 adopted dihedral angles of a right-handed α-helix, while in the holo-enzyme these same ϕ, ψ angles fell into the left-handed helical region of the Ramachandran plot. The net result of these changes was that the two polypeptide chains headed off into completely different directions after Asp 301. The backbones for the apo- and holo-enzymes matched up again at Pro 322. In the next X-ray study of phosphotriesterase, the Zn^{2+}/Zn^{2+}-substituted enzyme was crystallized and its structure solved to 2.1 Å resolution (*9*). Unlike that observed for the cadmium-containing enzyme, this time diethyl 4-methylbenzyl phosphonate was observed binding in the active site.

In the four structures presented here, the metal ion located in the β-site is surrounded in an octahedral coordination sphere in the cadmium-, the mixed cadmium/zinc-, and the manganese-containing phosphotriesterases. With the zinc-form, however, the coordination sphere fluctuates between trigonal bipyramidal as in the model described here or in the structure with bound diisopropyl methyl phosphonate (*12*) or tetrahedral as observed in complexes of the enzyme with

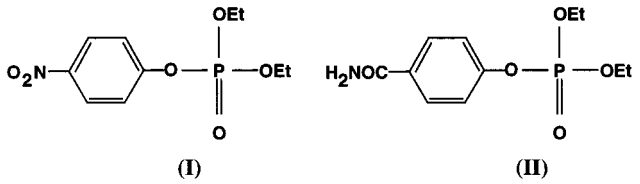

FIGURE 8: Substrates for phosphotriesterase.

Scheme 2

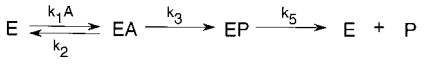

either diethyl 4-methylbenzyl phosphonate or triethyl phosphate (*9*, *12*). Phosphotriesterase accommodates these different metals in the β-position by simply filling in the coordination sphere with water molecules. It will be of interest to determine the three-dimensional structures of the various metal-substituted forms of phosphotriesterase in the presence of additional substrate analogues. This work is in progress.

The metal-substituted variants of phosphotriesterase had been previously analyzed for their ability to hydrolyze a library of organophosphate triesters possessing leaving-group phenols with pK_a values ranging from 4 to 10 (*17*). These studies demonstrated that the rate-limiting step for the enzyme-catalyzed hydrolysis of these compounds changes from phosphorus−oxygen bond cleavage (k_3) to a step associated with product release and regeneration of free enzyme (k_5) as the pK_a of the leaving-group phenol is diminished. The Brønsted plots showed that this transition in rate-limiting steps occurs with leaving-group phenols having pK_a values ~7.8−8.0 (*17*). The minimal kinetic mechanism that can be written for phosphotriesterase is presented in Scheme 2 where E is the free enzyme, while A and P represent the substrate and two products, respectively. With the substrate paraoxon, compound **I** in Figure 8, the *p*-nitrophenol leaving-group has a pK_a of 7.1, and the k_{cat} values for the Zn^{2+}/Zn^{2+}-, Cd^{2+}/Cd^{2+}-, Mn^{2+}/Mn^{2+}-, and Zn^{2+}/Cd^{2+}-substituted forms of the enzyme are 2200, 12 900, 4400, and 2600 s^{-1}, respectively (*17*). For the slower substrate, compound **II** in Figure 8, the leaving group has a pK_a of 8.6, and the k_{cat} values for the Zn^{2+}/Zn^{2+}-, Cd^{2+}/Cd^{2+}-, Mn^{2+}/Mn^{2+}-, and Zn^{2+}/Cd^{2+}-substituted forms of phosphotriesterase are 100, 730, 300, and 47 s^{-1}, respectively (*17*). Catalytic turnover of the slow substrate is predominantly limited by the chemical rate of P−O bond cleavage. This conclusion is experimentally supported by the large primary ^{18}O kinetic isotope effect of 1.036 (*18*−*19*).

With paraoxon, the rate-limiting step for all of the metal-substituted variants of phosphotriesterase is after P−O bond cleavage. This conclusion is also supported by the very low ^{18}O kinetic isotope effect of 1.002 for paraoxon (*18*−*19*). In the minimal Scheme 2, this transformation is depicted as product release and regeneration of free enzyme. However, this step also includes a recharging of the nucleophilic water molecule, which bridges the binuclear metal center of the enzyme. When the rate-limiting step for k_{cat} changes from bond cleavage to product release, phosphotriesterase also displays a distinctive dependence on the rate of the reaction with the identity of the metals comprising the binuclear metal center. The value of k_{cat} for paraoxon is larger with cadmium and smaller with zinc. Again, the value of k_{cat} with the fast substrate paraoxon for the Zn^{2+}/Cd^{2+}-hybrid is very much like the Zn^{2+}/Zn^{2+}-substituted form of the enzyme. Thus the structural position occupied by the zinc in the Zn^{2+}/Cd^{2+}-hybrid dominates this step in the catalytic mechanism (k_5) and in actual bond cleavage (k_3).

What is not clearly defined from a comparison of the structural studies reported here and the previous mechanistic investigations is why the Cd^{2+}/Cd^{2+}-substituted phosphotriesterase has a k_{cat} for either substrate in Figure 8 (**I** and **II**) that is 6- to 7-fold faster than the Zn^{2+}/Zn^{2+}-protein. In contrast, the values of k_{cat}/K_m are 3- to 7-fold higher for the Zn^{2+}/Zn^{2+}-protein than for the Cd^{2+}/Cd^{2+}-phosphotriesterase with these same two substrates (*17*). These differences in rate may reflect, in part, the inherent chemical potentials by the individual metal ions and/or the subtle structural perturbations imposed on the binuclear metal center by the protein matrix and associated chemical environment. Nevertheless, the kinetic parameters for the Zn^{2+}/Cd^{2+}-hybrid are very much more like the Zn^{2+}/Zn^{2+}-enzyme than the Cd^{2+}/Cd^{2+}-protein and thus the zinc in the Zn^{2+}/Cd^{2+}-hybrid is dominating the catalytic activity of this metal variant of phosphotriesterase. Therefore, the positional identity of the cadmium and the zinc in the binuclear metal hybrid may enable a mechanistic distinction to be made for the individual roles of the two metal ions in the catalytic activity of the enzyme.

The structural identity of the Zn^{2+}/Cd^{2+}-mixed species was first examined by ^{113}Cd NMR spectroscopy (*5*). These studies demonstrated that only a single NMR resonance was observed at 115 ppm when ^{113}Cd was used to prepare the Zn^{2+}/Cd^{2+}-enzyme hybrid. In contrast, the Cd^{2+}/Cd^{2+}-phosphotriesterase exhibited single resonances at 116 and 212 ppm, and thus each cadmium in this metal complex experienced a different chemical environment. Since the resonance at 212 ppm disappeared in the Zn^{2+}/Cd^{2+}-hybrid while the resonance at ~116 ppm remained, the zinc in the hybrid must be occupying the specific site originally held by the cadmium that resonated at 212 ppm. At the time of these NMR investigations, the three-dimensional structure of phosphotriesterase was unknown and thus it was not possible to assign a specific metal to an individual site within the binuclear metal center.

Recently, an ab initio determination of the structure of the binuclear metal center of phosphotriesterase was completed by Kafafi and Krauss (*20*). They predicted the sites of occupancy of the zinc and cadmium ions within the Zn^{2+}/Cd^{2+}-hybrid species based on the previously determined X-ray structure of the Zn^{2+}/Zn^{2+}-form (*9*). Their conclusion was that the cadmium was bound to the α-site while the zinc was bound to the β-site. These assignments were rationalized, in part, on the added stability expected for the larger cadmium at the five-coordinate site that is more buried and the smaller zinc at the more solvent-exposed site that is four-coordinate. However, these calculations apparently neglected, to some extent, the tendency of the more solvent-exposed β-site to expand its inner-sphere ligands with added water molecules. If one takes note of the fact that the β-site within the binuclear metal center is actually octahedral for the Cd^{2+}/Cd^{2+}-, Mn^{2+}/Mn^{2+}-, and Zn^{2+}/Cd^{2+}-enzymes, then these same arguments suggest that in the Zn^{2+}/Cd^{2+}-hybrid, the zinc would preferentially occupy the five-coordinate solvent-shielded site, while the cadmium would reside in the six-coordinate β-site.

Scheme 3

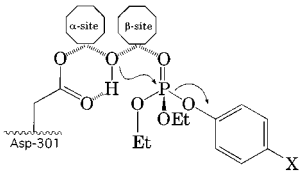

A working model for the initial catalytic complex that shows the binding orientation of the substrate with the binuclear metal center is presented in Scheme 3. In this model, the phosphoryl-oxygen bond is polarized through its association with the metal ion at the β-site. Support for this particular feature of the model comes from the structure of Zn^{2+}/Zn^{2+}-phosphotriesterase with the bound inhibitor diisopropyl methyl phosphonate, a sarin mimic (*12*). Nucleophilic attack would occur from the water or hydroxide ion that bridges the two metal ions and that is apparently hydrogen bonded to the carboxylate of Asp 301. The binuclear metal center in phosphotriesterase helps to catalyze the hydrolysis of organophosphates through activation of the bridging solvent molecule and polarization of the phosphoryl oxygen bond. The activation of the bridging solvent molecule by the α-site metal ion is apparently the dominant catalytic feature of the binuclear metal center. Thus far, there is no structural or mechanistic support for charge neutralization of the leaving group phenol via proton transfer or Lewis acid catalysis.

ACKNOWLEDGMENT

We gratefully acknowledge the helpful discussions of Dr. W. W. Cleland. Use of the Argonne National Laboratory Structural Biology Center beamlines at the Advanced Photon Source was supported by the U. S. Department of Energy, Office of Energy Research, under contract no. W-31-109-ENG-38.

REFERENCES

1. Dumas, D. P., Caldwell, S. R., Wild, J. R., and Raushel, F. M. (1989) *J. Biol. Chem. 264*, 19659−19665.
2. Donarski, W. J., Dumas, D. P., Heitmeyer, D. P., Lewis, V. E., and Raushel, F. M. (1989) *Biochemistry 28*, 4650−4655.
3. Dumas, D. P., Durst, H. D., Landis, W. G., Raushel, F. M., and Wild, J. R. (1990) *Arch. Biochem. Biophys. 277*, 155−159.
4. Chae, M. Y., Omburo, G. A., Lindahl, P. A., and Raushel, F. M. (1993) *J. Am. Chem. Soc. 115*, 12173−12174.
5. Omburo, G. A., Mullins, L. S., and Raushel, F. M. (1993) *Biochemistry 32*, 9148−9155.
6. Omburo, G. A., Kuo, J. M., Mullins, L. S., and Raushel, F. M. (1992) *J. Biol. Chem. 267*, 13278−13283.
7. Benning, M. M., Kuo, J. M., Raushel, F. M., and Holden, H. M. (1994) *Biochemistry 33*, 15001−15007.
8. Benning, M. M., Kuo, J. M., Raushel, F. M., and Holden, H. M. (1995) *Biochemistry 34*, 7973−7978.
9. Vanhooke, J. L., Benning, M. M., Raushel, F. M., and Holden, H. M. (1996) *Biochemistry 35*, 6020−6025.
10. Jabri, E., Carr, M. B., Hausinger, R. P., and Karplus, P. A. (1995) *Science 268*, 998−1004.
11. Lewis, V. E., Donarski, W. J., Wild, J. R., and Raushel, F. M. (1988) *Biochemistry 27*, 1591−1597.
12. Benning, M. M., Hong, S.-B., Raushel, F. M., and Holden, H. M. (2000) *J. Biol. Chem. 275*, 30556−30560.
13. Otwinowski, Z., and Minor, W. (1997) *Methods Enzymol. 276*, 307−326.
14. Tronrud, D. E., Ten Eyck, L. F., and Matthews, B. W. (1987) *Acta Crystallogr. Sect. A. 43*, 489−501.
15. Roussel, A., and Cambillau, C. (1991) in *Silicon Graphics Geometry Partners Directory*, Silicon Graphics.
16. Kleywegt, G. J., and Jones, T. A. (1996) *Acta Crystallogr. D52*, 826−828.
17. Hong, S.-B., Raushel, F. M. (1996) *Biochemistry 35*, 10904−10912.
18. Caldwell, S. R., Raushel, F. M., Weiss, P. M., and Cleland, W. W. (1991) *J. Am. Chem. Soc. 113*, 730−732.
19. Caldwell, S. R., Raushel, F. M., Weiss, P. M., and Cleland, W. W. (1991) *Biochemistry 30*, 7444−7450.
20. Kafafi, S., and Krauss, M. (1999) *Int. J. Quantum Chem. 75*, 289−299.
21. Kraulis, P. J. (1991) *J. Appl. Crystallogr. 24*, 946−950.

BI002661E